

Multiple scattering by random particulate media: exact 3D results

Michael I. Mishchenko^{1*}, Li Liu¹, Daniel W. Mackowski²,
Brian Cairns¹, and Gorden Videen³

¹NASA Goddard Institute for Space Studies, 2880 Broadway, New York, NY 10025

²Department of Mechanical Engineering, 201 Ross Hall, Auburn University, AL 36849-5341

³US Army Research Laboratory, AMSRD-ARL-CI-EM, 2800 Powder Mill Road, Adelphi, MD 20783-1197

*mmishchenko@giss.nasa.gov

Abstract: We use the numerically exact superposition T -matrix method to perform extensive computations of electromagnetic scattering by a 3D volume filled with randomly distributed wavelength-sized particles. These computations are used to simulate and analyze the effect of randomness of particle positions as well as the onset and evolution of various multiple-scattering effects with increasing number of particles in a statistically homogeneous volume of discrete random medium. Our exact results illustrate and substantiate the methodology underlying the microphysical theories of radiative transfer and coherent backscattering. Furthermore, we show that even in densely packed media, the light multiply scattered along strings of widely separated particles still provides a significant contribution to the total scattered signal and thereby makes quite pronounced the classical radiative transfer and coherent backscattering effects.

©2007 Optical Society of America

OCIS codes: (030.1670) Coherent optical effects; (030.5620) Radiative transfer; (030.6140) Speckle; (290.4210) Multiple scattering; (290.5850) Scattering, particles.

References and links

1. A. Ishimaru, *Wave Propagation and Scattering in Random Media* (Academic Press, New York, 1978).
2. V. L. Kuz'min and V. P. Romanov, "Coherent phenomena in light scattering from disordered systems," *Phys.–Uspekhi* **39**, 231–260 (1996).
3. E. Amic, J. M. Luck, and T. M. Nieuwenhuizen, "Multiple Rayleigh scattering of electromagnetic waves," *J. Phys. I (France)* **7**, 445–483 (1997).
4. M. C. W. van Rossum and T. M. Nieuwenhuizen, "Multiple scattering of classical waves: microscopy, mesoscopy, and diffusion," *Rev. Mod. Phys.* **71**, 313–371 (1999).
5. L. Tsang and J. A. Kong, *Scattering of Electromagnetic Waves: Advanced Topics* (Wiley, New York, 2001).
6. P. Sebbah, ed., *Waves and Imaging through Complex Media* (Springer, Berlin, 2001).
7. V. V. Tuchin, ed., *Handbook of Optical Biomedical Diagnostics* (SPIE Press, Bellingham, Wa., 2002).
8. B. A. van Tiggelen and S. E. Skipetrov, eds., *Wave Scattering in Complex Media: From Theory to Applications* (Springer, Berlin, 2003).
9. J. W. Hovenier, C. van der Mee, and H. Domke, *Transfer of Polarized Light in Planetary Atmospheres – Basic Concepts and Practical Methods* (Springer, Berlin, 2004).
10. G. Videen, Ya. Yatskiv, and M. Mishchenko, eds., *Photopolarimetry in Remote Sensing* (Springer, Berlin, 2004).
11. M. I. Mishchenko, L. D. Travis, and A. A. Lacis, *Multiple Scattering of Light by Particles: Radiative Transfer and Coherent Backscattering* (Cambridge U. Press, Cambridge, UK, 2006).
12. S. H. Tseng, Y. L. Kim, A. Taflove, D. Maitland, V. Backman, and J. T. Walsh, Jr., "Simulation of enhanced backscattering of light by numerically solving Maxwell's equations without heuristic approximations," *Opt. Express* **13**, 3666–3672 (2005).
13. S. H. Tseng, A. Taflove, D. Maitland, and V. Backman, "Pseudospectral time domain simulations of multiple light scattering in three-dimensional macroscopic random media," *Radio Sci.* **41**, RS4009 (2006).
14. D. W. Mackowski, "Direct simulation of scattering and absorption by particle deposits," *Proc. IMECE* **2006**, 14615 (2006).
15. M. I. Mishchenko and L. Liu, "Weak localization of electromagnetic waves by densely packed many-particle groups: exact 3D results," *J. Quant. Spectrosc. Radiat. Transfer*, doi:10.1016/j.jqsrt.2007.01.039 (2007).

16. D. W. Mackowski and M. I. Mishchenko, "Calculation of the T matrix and the scattering matrix for ensembles of spheres," *J. Opt. Soc. Am. A* **13**, 2266–2278 (1996).
17. M. I. Mishchenko, L. D. Travis, and A. A. Lacis, *Scattering, Absorption, and Emission of Light by Small Particles* (Cambridge U. Press, Cambridge, UK, 2002). <http://www.giss.nasa.gov/~crimim/books.html>.
18. D. Mackowski, K. Fuller, and M. Mishchenko, "Codes for calculation of scattering by clusters of spheres." <ftp://ftp.eng.auburn.edu/pub/dmckowski/scatcodes/index.html>.
19. M. I. Mishchenko, G. Videen, V. A. Babenko, N. G. Khlebtsov, and T. Wriedt, " T -matrix theory of electromagnetic scattering by particles and its applications: a comprehensive reference database," *J. Quant. Spectrosc. Radiat. Transfer* **88**, 357–406 (2004).
20. W. Brown, ed., *Dynamic Light Scattering* (Clarendon Press, Oxford, UK, 1993).
21. S. Etemad, R. Thompson, and M. J. Andrejco, "Weak localization of photons: universal fluctuations and ensemble averaging," *Phys. Rev. Lett.* **57**, 575–578 (1986).
22. D. W. Mackowski, "A simplified model to predict the effects of aggregation on the absorption properties of soot particles," *J. Quant. Spectrosc. Radiat. Transfer* **100**, 237–249 (2006).
23. P. H. Kaye, K. Aptowicz, R. K. Chang, V. Foot, and G. Videen, "Angularly resolved elastic scattering from airborne particles," in *Optics of Biological Particles*, A. Hoekstra, V. Maltsev, and G. Videen, eds. (Springer, Berlin, 2007), pp. 31–60.
24. P. A. Martin, *Multiple Scattering: Interaction of Time-Harmonic Waves with N Obstacles* (Cambridge U. Press, Cambridge, UK, 2006).
25. S. Etemad, R. Thompson, M. J. Andrejco, S. John, and F. C. MacKintosh, "Weak localization of photons: termination of coherent random walks by absorption and confined geometry," *Phys. Rev. Lett.* **59**, 1420–1423 (1987).
26. F. T. Ulaby and C. Elachi, eds., *Radar Polarimetry for Geoscience Applications* (Artech House, Norwood, Mass., 1990).
27. S. J. Ostro, "Planetary radar astronomy," *Rev. Mod. Phys.* **65**, 1235–1279 (1993).
28. B. A. Campbell, *Radar Remote Sensing of Planetary Surfaces* (Cambridge U. Press, Cambridge, UK, 2002).
29. M. I. Mishchenko, "On the nature of the polarization opposition effect exhibited by Saturn's rings," *Astrophys. J.* **411**, 351–361 (1993).
30. M. P. van Albada, M. B. van der Mark, and A. Lagendijk, "Polarization effects in weak localization of light," *J. Phys. D: Appl. Phys.* **21**, S28–S31 (1988).
31. K. Muinonen, "Coherent backscattering of light by complex random media of spherical scatterers: numerical solution," *Waves Random Media* **14**, 365–388 (2004).
32. V. P. Tishkovets and M. I. Mishchenko, "Coherent backscattering of light by a layer of discrete random medium," *J. Quant. Spectrosc. Radiat. Transfer* **86**, 161–180 (2004).
33. N. T. Zakharova and M. I. Mishchenko, "Scattering properties of needlelike and platelike ice spheroids with moderate size parameters," *Appl. Opt.* **39**, 5052–5057 (2000).
34. N. T. Zakharova and M. I. Mishchenko, "Scattering by randomly oriented thin ice disks with moderate equivalent-sphere size parameters," *J. Quant. Spectrosc. Radiat. Transfer* **70**, 465–471 (2001).
35. V. K. Rosenbush, V. V. Avramchuk, A. E. Rosenbush, and M. I. Mishchenko, "Polarization properties of the Galilean satellites of Jupiter: observations and preliminary analysis," *Astrophys. J.* **487**, 402–414 (1997).
36. M. I. Mishchenko, V. K. Rosenbush, and N. N. Kiselev, "Weak localization of electromagnetic waves and opposition phenomena exhibited by high-albedo atmosphereless solar system objects," *Appl. Opt.* **45**, 4459–4463 (2006).
37. E. Zubko, Yu. Shkuratov, M. Hart, J. Eversole, and G. Videen, "Backscattering and negative polarization of agglomerate particles," *Opt. Lett.* **28**, 1504–1506 (2003).
38. E. Zubko, Yu. Shkuratov, M. Hart, J. Eversole, and G. Videen, "Backscattering of agglomerate particles," *J. Quant. Spectrosc. Radiat. Transfer* **88**, 163–171 (2004).
39. V. P. Tishkovets, P. V. Litvinov, and M. V. Lyubchenko, "Coherent opposition effects for semi-infinite discrete random medium in the double-scattering approximation," *J. Quant. Spectrosc. Radiat. Transfer* **72**, 803–811 (2002).
40. P. Litvinov, V. Tishkovets, and K. Ziegler, "Coherent backscattering effects for discrete random media," *J. Quant. Spectrosc. Radiat. Transfer* **103**, 131–145 (2007).
41. Yu. Shkuratov, S. Bondarenko, A. Ovcharenko, C. Pieters, T. Hiroi, H. Volten, O. Muñoz, and G. Videen, "Comparative studies of the reflectance and degree of linear polarization of particulate surfaces and independently scattering particles," *J. Quant. Spectrosc. Radiat. Transfer* **100**, 340–358 (2006).
42. A. Ovcharenko, S. Bondarenko, Yu. Shkuratov, C. Scotto, C. Merritt, M. Hart, J. Eversole, and G. Videen, "Backscatter effects of surfaces composed of dry biological particles," *J. Quant. Spectrosc. Radiat. Transfer* **101**, 462–470 (2006).
43. D. S. Wiersma, P. Bartolini, A. Lagendijk, and R. Righini, "Localization of light in a disordered medium," *Nature* **390**, 671–673 (1997).
44. F. Scheffold, R. Lenke, R. Tweer, and G. Maret, "Localization or classical diffusion of light?" *Nature* **398**, 206–207 (1999).
45. D. S. Wiersma, J. G. Rivas, P. Bartolini, A. Lagendijk, and R. Righini, "Localization or classical diffusion of light? Reply," *Nature* **398**, 207 (1999).

46. A. A. Chabanov, M. Stoytchev, and A. Z. Genack, "Statistical signatures of photon localization," *Nature* **404**, 850–853 (2000).
 47. M. Störzer, P. Gross, C. M. Aegerter, and G. Maret, "Observation of the critical regime near Anderson localization of light," *Phys. Rev. Lett.* **96**, 063904 (2006).
-

1. Introduction

Multiple scattering of electromagnetic waves by macroscopic media composed of randomly positioned particles is a subject of great importance to many science and engineering disciplines. Until quite recently, the only practical means of multiple-scattering computations for turbid and other particulate media have been various approximate approaches such as the effective field approximation, the quasi-crystalline approximation, the diffusion approximation, the radiative transfer theory (RTT), the phenomenological and microphysical theories of coherent backscattering (CB), and the phenomenological theory of strong localization [1–11]. However, the ever increasing power of scientific workstations and the availability of efficient numerical techniques have recently led to the emergence of an accurate quantitative approach to this complex problem based on direct computer solutions of the Maxwell equations [12–15]. For practical reasons, this approach cannot be used yet to simulate electromagnetic scattering by random media consisting of extremely large numbers of particles such as clouds, colloids, and powder surfaces. However, it does provide the potential to model rather complex particulate systems and determine all quantitative scattering characteristics some of which may not be straightforward to measure accurately. Therefore, this approach can be used to evaluate the predictions and conditions of applicability of an approximate theory.

The objective of this paper is to use numerically exact solutions of the Maxwell equations in order to simulate the effect of randomness of particle positions and the onset and evolution of multiple-scattering effects with increasing number of particles randomly distributed throughout a finite scattering volume. This allows us to model and analyze the specific scattering regimes that are encountered in such disciplines as dynamic light scattering, RTT, and the theory of CB.

All numerical results described in this paper have been obtained with the highly efficient superposition *T*-matrix method (STMM) [16, 17]. The corresponding computer codes are publicly available on the World Wide Web [18] and yield all scattering and absorption characteristics of a multi-sphere group in fixed and random orientations. The codes have been tested thoroughly and give very accurate results within the domain of numerical convergence. Although STMM has been used extensively in computations for particle aggregates such as fractal clusters composed of touching soot or mineral monomers [19], the approach adopted for this paper is to model specifically light scattering by a statistically homogeneous volume of particulate medium. Keeping the size of the volume fixed and gradually increasing the number of randomly distributed particles allows us to perform a systematic analysis of emerging and intensifying multiple-scattering effects and thereby illustrate and substantiate the specific assumptions used in the microphysical derivation of the radiative transfer equation (RTE) and in the microphysical theory of CB [11].

In order to avoid redundancy and save space, we take advantage of the on-line availability of [17] and use exactly the same terminology and notation.

2. Static and dynamic light scattering

As shown in Fig. 1, we assume that a number of identical spherical particles are distributed randomly throughout a spherical volume V with a radius R much greater than the particle radius r . We have fixed the size parameter of the particles at $k_1 r = 4$, where k_1 is the wave number in the surrounding medium; whereas, the size parameter of the spherical volume has been fixed at $k_1 R = 40$. The number of particles in the spherical volume N is varied between 1 and 240, thereby yielding particle volume concentrations ranging from 0.1% to 24%. Note that the size of the scattering volume and the maximal number of particles do not represent

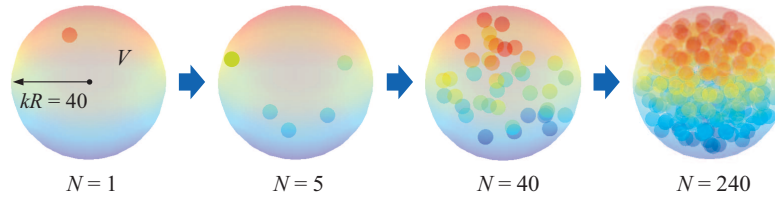


Fig. 1. Spherical scattering volume V filled with N randomly positioned particles.

inherent limitations of STMM but rather are constrained by the efficiency and memory size of the computer used.

Solving the macroscopic Maxwell equations yields the electromagnetic field scattered by a stationary object [11, 17]. This is sufficient if one considers the scattering of monochromatic light (e.g., laser light) by a fixed object that does not move with respect to the source of light and the detector during the measurement. However, to simulate measurements of light scattering by a rapidly changing object, one needs to solve the Maxwell equations repeatedly for a representative set of distinct object configurations. This applies equally to a cloud or suspension of independently moving particles [11, 20] and to a bound multi-particle group (e.g., particulate surface) that moves as a whole with respect to the source of light and/or the detector [21].

After the set of solutions of the Maxwell equations has been obtained, one has a choice of analyzing the statistical information content of differences in the individual solutions or applying an averaging procedure and thereby isolating the static component of the scattering pattern. These two approaches are traditionally referred to as *dynamic* and *static* light scattering [11, 20].

To model numerically dynamic light scattering by a statistically homogeneous volume of random particulate medium, one needs a procedure that assigns coordinates to particles forming a specific realization of the random N -particle group filling the volume. In our computations, we have used interchangeably two independent approaches. The first one employs a random-number generator to assign sequentially 3D coordinates to each of the N particles in a trial-and-error fashion ensuring that the particles do not overlap. We refer to this procedure as Random Coordinate Generator 1 (RCG-1). The second one, hereinafter referred to as RCG-2, is a modification of the procedure described in [22] wherein the fractal dimension of the N -particle group is set at 3 and each newly added particle is not required to be in direct contact with at least one already existing particle. For example, the specific $N = 1$ and 5 configurations in Fig. 1 were generated with RCG-1, whereas the $N = 40$ and 240 configurations were generated with RCG-2.

To simulate static light scattering, one needs an efficient way of averaging the computed scattering signal over very many different configurations of the N -particle group. One can, of course, use RCG-1 or RCG-2 repeatedly to create a large number of different N -particle configurations and then average the corresponding T -matrix results numerically. The approach adopted for this study has been to create only one random N -particle configuration and then to average over all possible orientations of this configuration with respect to the laboratory coordinate system. This procedure yields in effect an infinite continuous set of random realizations of the N -particle group and takes full advantage of the highly efficient semi-analytical orientation averaging procedure afforded by STMM [16, 17].

Although natural and man-made particles exhibit a virtually endless variety of refractive indices, we have made this research project practicable by selecting only two values. The first one, $m = 1.32$, is typical of both water and water ice at visible wavelengths, while the second one, $m = 1.5$, is representative of many minerals, glasses, and synthetic materials.

3. Fixed configurations of randomly positioned particles: speckle

We assume that the large spherical volume V is illuminated by a plane electromagnetic wave or a parallel quasi-monochromatic beam of light propagating in the direction $\hat{\mathbf{n}}^{\text{inc}}$ (Fig. 2).

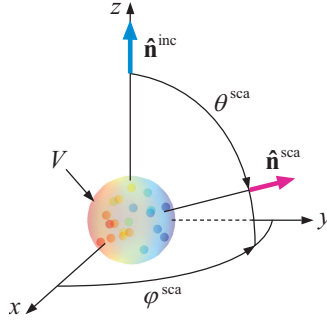


Fig. 2. Electromagnetic scattering by a volume V of discrete random medium. In this case the scattering volume is filled with 20 randomly positioned particles.

The angular distribution and polarization state of the scattered light in the far-field zone of the entire scattering volume is fully described by the Stokes phase matrix \mathbf{Z} . The latter specifies the transformation of the Stokes parameters of the incident light into those of the light scattered in the observation direction $\hat{\mathbf{n}}^{\text{sca}}$ [17]:

$$\begin{bmatrix} I^{\text{sca}} \\ Q^{\text{sca}} \\ U^{\text{sca}} \\ V^{\text{sca}} \end{bmatrix} \propto \mathbf{Z}(\hat{\mathbf{n}}^{\text{sca}}, \hat{\mathbf{n}}^{\text{inc}}) \begin{bmatrix} I^{\text{inc}} \\ Q^{\text{inc}} \\ U^{\text{inc}} \\ V^{\text{inc}} \end{bmatrix}. \quad (1)$$

The Stokes parameters of the incident and scattered light are defined with respect to the corresponding meridional planes. We always assume that the incidence direction coincides with the positive direction of the z -axis of the laboratory reference frame and that the meridional plane of the incidence direction coincides with the xz half-plane with $x \geq 0$.

Let us first assume that the incident light is circularly polarized in the counter-clockwise sense when viewed in the direction of propagation, which implies that $V^{\text{inc}} = I^{\text{inc}}$ and $Q^{\text{inc}} = U^{\text{inc}} = 0$. Panels (a)–(e) of Fig. 3 show the far-field angular distributions of the total intensity, I^{sca} , scattered in the backward hemisphere by the large spherical volume filled with $N = 1, 5, 20, 40,$ and 80 particles having the same refractive index $m = 1.32$. The individual particle positions are chosen randomly using RCG-1, but otherwise they are fixed. The scattering pattern for $N = 1$ is rather smooth and perfectly azimuthally symmetric, as it should be for a single wavelength-sized spherical particle. However, the other panels demonstrate typical speckle patterns of increasing complexity.

The interference origin of the speckle is illustrated in Fig. 4(a). It is known that a convenient exact means of describing electromagnetic scattering by an arbitrary multi-particle group is afforded by the so-called Foldy–Lax equations (FLEs) which allow the decomposition of the total scattered field into individual-particle contributions (see Section 4.1 of [11]). Furthermore, FLEs can be cast into an order-of-scattering form which allows the interpretation of the total scattered field as consisting of partial fields resulting from the incident wave being scattered along all possible particle sequences. Two such sequences are shown in Fig. 4(a). At an observation point located in the far-field zone of the entire scattering volume, the corresponding field contributions become outgoing spherical wavelets and interfere, the result of the interference being dependent on the phase difference between the wavelets. If the interference is constructive (destructive) then it serves to increase (decrease) the total intensity scattered in the direction $\hat{\mathbf{n}}^{\text{sca}}$. The total intensity is the sum of the interference results evaluated for all possible pairs of scattering sequences. The typical angular width of each interference maximum or minimum is proportional to $1/k_1 \langle d \rangle$, where $\langle d \rangle$ is the average distance between the particles; whereas, the number of these maxima and

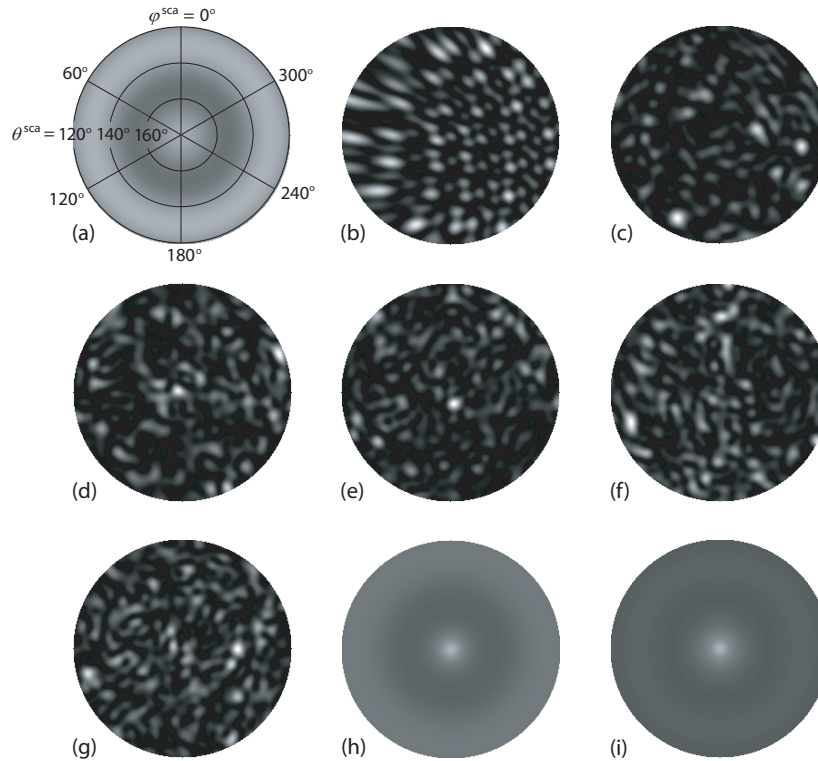


Fig. 3. Angular distribution of scattered intensity in the far-field zone of the spherical volume V filled with N particles. (a) $N = 1$ and $m = 1.32$. (b) $N = 5$ and $m = 1.32$. (c) $N = 20$ and $m = 1.32$. (d) $N = 40$ and $m = 1.32$. (e) $N = 80$ and $m = 1.32$. (f) $N = 80$ and $m = 1.32$. (g) $N = 80$ and $m = 1.5$. (h) $N = 80$ and $m = 1.32$, random orientation. (i) $N = 80$ and $m = 1.5$, random orientation. The gray scale was individually adjusted in order to maximally reveal the details of each scattering pattern. Panel (a) also shows the angular coordinates used for all panels.

minima grows swiftly with increasing N . These two factors explain the spotty appearance and the rapidly increasing complexity of the scattering patterns in panels 3(b)–3(e).

Of course, the speckle pattern depends not only on the number of particles N but also on the specific way they are arranged with respect to the laboratory coordinate system. This is illustrated by panels 3(e) and 3(f) computed for two different, random 80-particle configurations shown in Fig. 5. The equally strong dependence of the speckle pattern on the particle refractive index is demonstrated by panels 3(e) and 3(g) computed for the same 80-particle configuration shown in Fig. 5(a) but for different refractive indices (1.32 and 1.5).

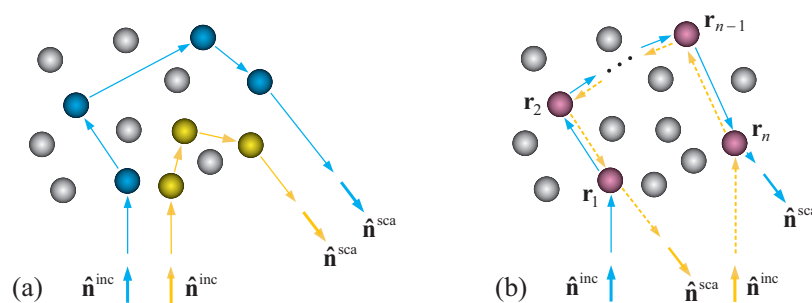


Fig. 4. Interference origin of (a) speckle and (b) coherent backscattering.

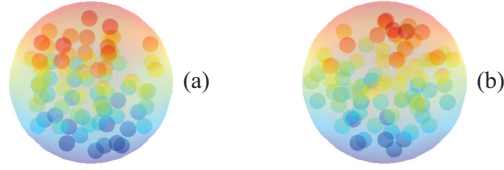


Fig. 5. Two random realizations of the 80-particle group created with (a) RCG-1 and (b) RCG-2.

The interference explanation of the speckle given above is valid for any fixed particle configuration, either sparsely or densely packed. Furthermore, FLEs are quite general and can be applied to any partitioning of a scattering object into components, which makes the interference explanation of the speckle valid for single-body scatterers as well as for multi-particle configurations. The universal nature of the speckle and its strong dependence on the refractive index and morphology of the scattering object explain the widespread use of speckle measurements for particle characterization (e.g., [23] and references therein). Statistical analyses of the speckle produced by dilute and optically thick particle suspensions form the basis of the disciplines called photon correlation spectroscopy and diffusing wave spectroscopy and are used to determine various particle characteristics such as velocity, size, and dispersity [6, 20].

4. Static scattering

Panels (e) and (f) of Fig. 3 illustrate the range of variability of the speckle pattern that can be expected upon even minute changes in a random multi-particle configuration. Obviously, neither the speckle pattern nor its variability are reproduced by the classical theories of radiative transfer and CB, which indicates that neither RTT nor the theory of CB describe the instantaneous state of electromagnetic radiation in a discrete random medium. Instead, both theories fall in the realm of static scattering and describe the result of averaging the relevant optical observables over a significant period of time or, equivalently, over a significant range of random particle positions [11].

To illustrate this fundamental point, panels (h) and (i) of Fig. 3 show the result of averaging the speckle pattern over the uniform orientation distribution of the 80-particle configuration depicted in Fig. 5(a) for $m = 1.32$ and $m = 1.5$, respectively. As one would expect on the basis of RTT considerations, both intensity distributions are perfectly azimuthally symmetric and rather smooth. The only notable feature common to both panels is the intensity peak centered at exactly the backscattering direction. We demonstrate below that this feature is caused by the CB effect.

5. Multiple scattering by a volume of discrete random medium

One does not need to assume that multiple interparticle scattering is an actual physical phenomenon taking place when an electromagnetic wave is scattered by a multi-particle group. Indeed, it follows from the Maxwell equations that at each moment the incident plane wave perceives the entire N -particle group as a single, albeit morphologically complex scatterer. However, as we already demonstrated in Section 3, the *concept* of multiple scattering is a useful *interpretation* of the order-of-scattering representation of FLEs amenable to straightforward and easy visualization [11, 24]. This is especially true of the situations that allow the introduction of the concept of “independent scattering.” The latter implies that all particles are widely separated and move randomly during the time of the measurement (see page 201 of [11]) and is a cornerstone of RTT and the theory of CB.

In this section, we employ the concept of multiple scattering to interpret various effects of increasing the number of particles filling the scattering volume on the static scattering patterns obtained by averaging over all orientations of a random N -particle configuration with respect to the laboratory reference frame. We assume for the sake of simplicity that $\varphi^{\text{sca}} = 0$ and

characterize the scattering direction by the scattering angle $\Theta = \theta^{\text{sca}}$. Then the scattering process can be described in terms of the so-called normalized Stokes scattering matrix [9, 11, 17] given by

$$\begin{bmatrix} a_1(\Theta) & b_1(\Theta) & 0 & 0 \\ b_1(\Theta) & a_2(\Theta) & 0 & 0 \\ 0 & 0 & a_3(\Theta) & b_2(\Theta) \\ 0 & 0 & -b_2(\Theta) & a_4(\Theta) \end{bmatrix}. \quad (2)$$

The specific block-diagonal structure of this matrix is confirmed by the T -matrix results and is largely caused by averaging over the uniform orientation distribution of a multi-particle group coupled with sufficient randomness of particle positions throughout the scattering volume afforded by both RCG-1 and RCG-2. All scattering matrix elements denoted in Eq. (2) by a zero have been found to be at least an order of magnitude smaller than the smallest non-zero element (in the absolute-value sense). The (1,1) element, called the phase function, satisfies the following standard normalization condition:

$$\frac{1}{2} \int_0^\pi d\Theta \sin \Theta a_1(\Theta) = 1. \quad (3)$$

The results of our extensive T -matrix computations are summarized in Figs. 6 and 7. The computer time required to compute all scattering characteristics of an N -particle group in random orientation ranged from ~12 min for $N = 2$ to ~210 h for $N = 240$ on a Power Mac G5 workstation with 1GB of RAM and 2.50 GHz CPU speed.

The phase function describes the angular distribution of the scattered intensity provided that the incident light is unpolarized. The upper left-hand panels of Figs. 6 and 7 vividly demonstrate several fundamental consequences of increasing the number of particles in the scattering volume. First, the constructive interference of light singly scattered by the component particles in the exact forward direction causes a strong forward-scattering enhancement [17]. This feature is further detailed in Fig. 8(a) and is explained in Fig. 9. Indeed, the exact forward-scattering direction is unique in that the phase of the wavelets singly forward-scattered by all the particles in the volume is exactly the same irrespective of the specific particle positions (Fig. 9(a)). In the absence of multiple scattering, the constructive interference of these wavelets would lead to an increase of the forward-scattering phase function $a_1(0^\circ)$ by a factor of N . This increase does occur for $N = 2$ and 5, but then slows down, and by the time N reaches the value 160 the $a_1(0^\circ)$ value saturates. This behavior can be interpreted in terms of a multiple-scattering effect whereby particle 3 (see the right-hand particle sequence in Fig. 9(b)) “shades” particle 2 by attenuating the incident field exciting particle 2. This multiple-scattering effect leads to the exponential extinction law in the framework of RTT [11]. When essentially the entire cross section of the scattering volume is filled with particles, $a_1(0^\circ)$ can be expected to nearly reach the value computed in the framework of the geometrical optics approximation for the entire scattering volume, $a_1^{\text{GO}}(0^\circ) = (k_1 R)^2 / 2 = 800$, and this indeed happens for $N \geq 160$ for both $m = 1.32$ and $m = 1.5$, Fig. 8(a). Furthermore, the position of the first phase-function minimum also becomes N - and m -independent and very close to the diffraction prediction $\approx 5.5^\circ$. The extinction efficiency factor for the entire volume also saturates at a value that is within 10% of the geometrical-optics limit of 2.

The second consequence of increasing N is that the phase functions at scattering angles $30^\circ \leq \Theta \leq 170^\circ$ become progressively smooth and featureless. This trait again can be interpreted in RTT terms as a typical result of increasing the amount of multiple scattering whereby light undergoing many scattering events forgets the initial incidence direction $\hat{\mathbf{n}}^{\text{inc}}$ and is more likely to contribute equally to all exit directions $\hat{\mathbf{n}}^{\text{sca}}$ [11].

Third, the phase functions at scattering angles $\Theta > 170^\circ$ begin to develop a backscattering enhancement which becomes quite pronounced for $N \geq 160$ (see Figs. 8(c) and 8(e)). This

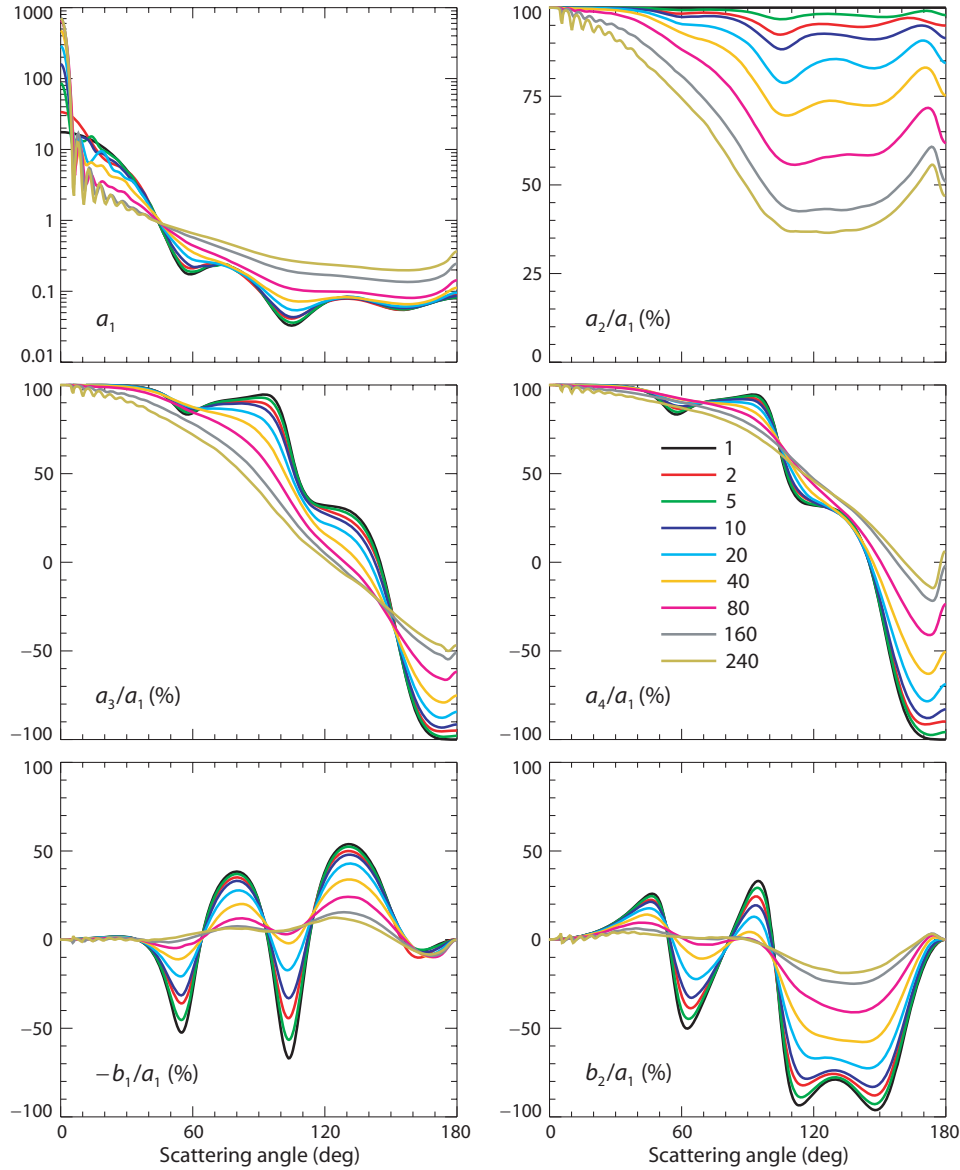


Fig. 6. Elements of the normalized Stokes scattering matrix computed for the volume V of discrete random medium filled with $N = 1, \dots, 240$ particles having the same refractive index $m = 1.32$.

feature has a refractive-index-independent angular width indicative of an interference origin [2, 4] and, as we will further substantiate, is a typical manifestation of CB. The standard explanation of the CB effect is illustrated by Fig. 4(b) and is as follows. The conjugate wavelets scattered along the same string of n particles but in opposite directions interfere, the interference being constructive or destructive depending on the phase difference

$$\Delta = k_1(\mathbf{r}_n - \mathbf{r}_1) \cdot (\hat{\mathbf{n}}^{\text{inc}} + \hat{\mathbf{n}}^{\text{sca}}). \quad (4)$$

If the observation direction $\hat{\mathbf{n}}^{\text{sca}}$ is far from the exact backscattering direction given by $-\hat{\mathbf{n}}^{\text{inc}}$ then the average effect of interference of the conjugate wavelets scattered along various strings of particles is zero, owing to the randomness of the particle positions. However, at

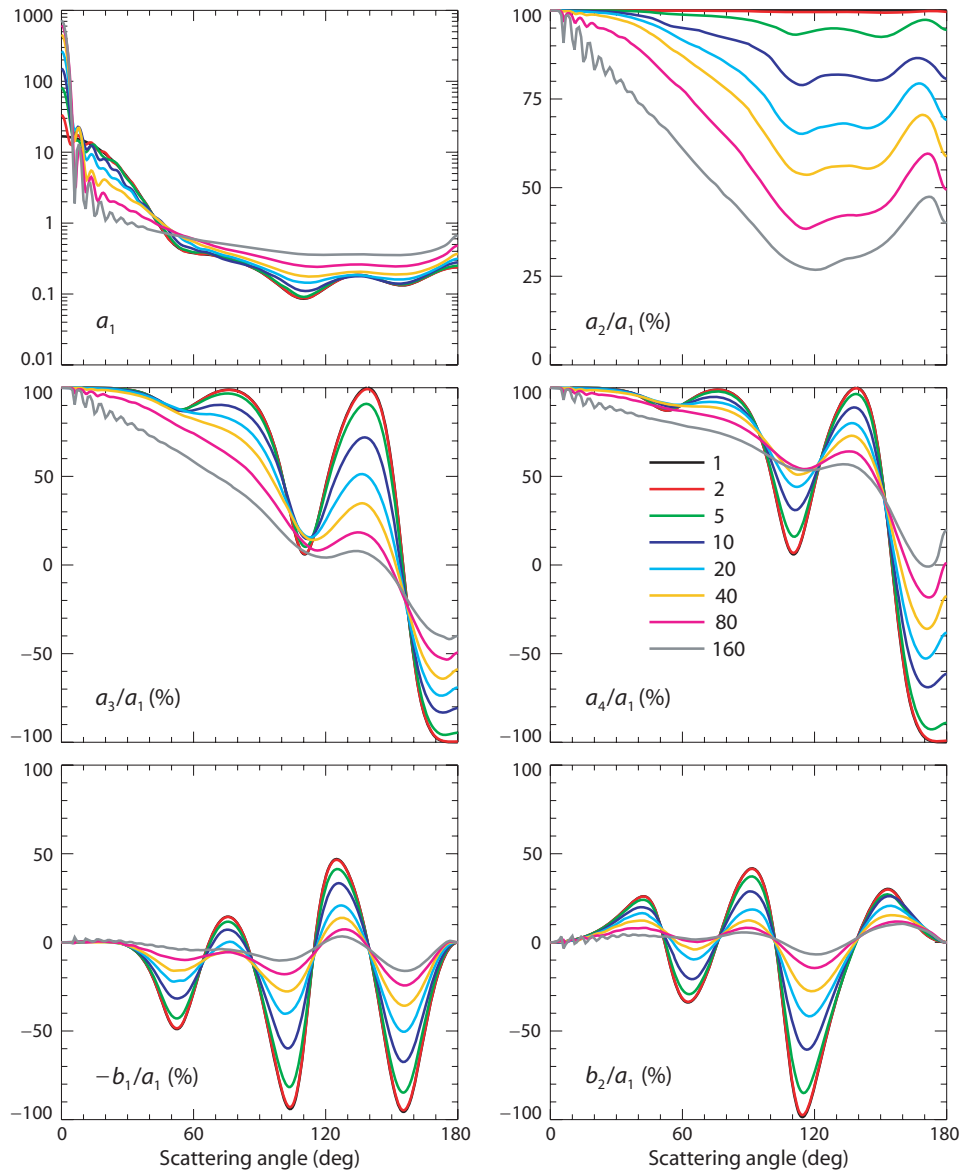


Fig. 7. Elements of the normalized Stokes scattering matrix computed for the volume V of discrete random medium filled with $N = 1, \dots, 160$ particles having the same refractive index $m = 1.5$.

exactly the backscattering direction, $\hat{\mathbf{n}}^{\text{sca}} = -\hat{\mathbf{n}}^{\text{inc}}$, the phase difference between the conjugate paths involving *any* string of particles is identically equal to zero, and the interference is always constructive and causes an intensity peak.

The ratio a_2/a_1 is identically equal to unity for scattering by a single sphere. Therefore, the rapidly growing deviation of this ratio from 100% for $N \geq 5$ can again be interpreted in RTT terms as a direct consequence of the strengthened depolarizing effect of multiple scattering (see Figs. 6 and 7). Similarly, $a_3(\Theta) \equiv a_4(\Theta)$ and $a_3(180^\circ)/a_1(180^\circ) = -1$ for single scattering by a spherically symmetric particle, but multiple scattering in particle groups with $N \geq 5$ causes an increasingly significant violation of these equalities.

The degree of linear polarization of the scattered light for unpolarized incident light is given by the ratio $-b_1/a_1$. The corresponding panels in Figs. 6 and 7 show that the most

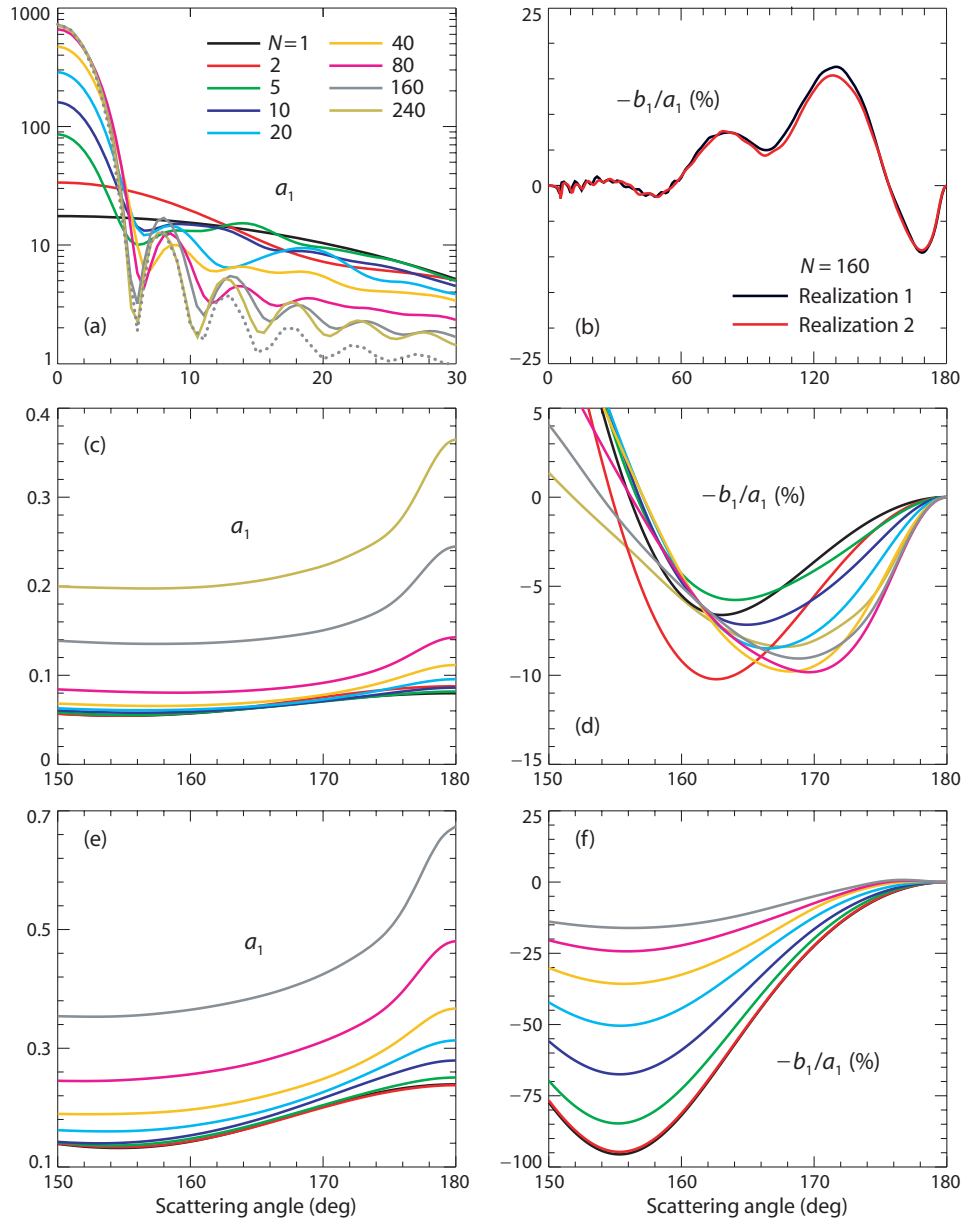


Fig. 8. Elements of the normalized Stokes scattering matrix computed for the volume V of discrete random medium filled with a varying number of particles. (a) $m = 1.32$ (solid curves) and 1.5 (dotted curve). (b) – (d) $m = 1.32$. (e) and (f) $m = 1.5$.

obvious effect of increasing N is to smooth out the oscillations in the polarization curve for the single wavelength-sized sphere and, on average, to make polarization more neutral. The standard RTT explanation of this trait is that the main contribution to the second Stokes parameter, Q^{sca} , comes from the first few orders of scattering; whereas, light scattered many times becomes largely unpolarized [9, 11].

If the incident light is polarized linearly in the scattering plane then $Q^{\text{inc}} = I^{\text{inc}}$ and $U^{\text{inc}} = V^{\text{inc}} = 0$. The corresponding angular distributions of the co-polarized,

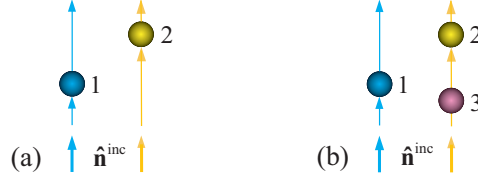


Fig. 9. Forward-scattering interference.

$$\frac{1}{2}(I^{\text{sca}} + Q^{\text{sca}}) \propto \frac{1}{2}[a_1(\Theta) + 2b_1(\Theta) + a_2(\Theta)], \quad (5)$$

and cross-polarized,

$$\frac{1}{2}(I^{\text{sca}} - Q^{\text{sca}}) \propto \frac{1}{2}[a_1(\Theta) - a_2(\Theta)], \quad (6)$$

scattered intensities are shown in Figs. 10 and 11. These figures also depict the same-helicity,

$$\frac{1}{2}(I^{\text{sca}} + V^{\text{sca}}) \propto \frac{1}{2}[a_1(\Theta) + a_4(\Theta)], \quad (7)$$

and opposite-helicity,

$$\frac{1}{2}(I^{\text{sca}} - V^{\text{sca}}) \propto \frac{1}{2}[a_1(\Theta) - a_4(\Theta)], \quad (8)$$

scattered intensities for the case of incident light polarized circularly in the counterclockwise direction when looking in the direction of propagation ($Q^{\text{inc}} = U^{\text{inc}} = 0$ and $V^{\text{inc}} = I^{\text{inc}}$). All of these quantities for both refractive indices exhibit CB in the form of backscattering peaks growing in amplitude with N .

By far the most unequivocal demonstration of the onset of CB is provided by the $(a_1 - a_2)/2$ and $(a_1 + a_4)/2$ curves in Figs. 10 and 11. Indeed, the corresponding single-particle curves show no backscattering enhancement at all, so the backscattering peaks that develop with increasing N (and thus with increasing amount of multiple scattering) can be attributed unequivocally to CB.

The amplitudes of all the backscattering intensity peaks in Figs. 8–10 (defined as the value at the exact backscattering direction divided by the nearby background value) never exceed 2 but can approach 2 very closely. The angular widths of these peaks are approximately the same, which also testifies to their common CB origin. All the peaks are rounded and have a zero derivative at $\Theta = 180^\circ$, as it should be for a finite scatterer [25]. Indeed, the triangular peak shape typical of semi-infinite nonabsorbing media [2, 4] is caused by extremely long scattering paths that provide interference contributions of infinitesimal angular width. In our case, the interference contribution from any string of particles cannot be narrower than that from the strings with the first and the last particle separated by $2R$ (cf. Eq. (4)), and this contribution already has a rounded profile at $\Theta = 180^\circ$.

Figures 10 and 11 also depict the angular profiles of the so-called linear, μ_L , and circular, μ_C , polarization ratios defined as the ratio of the cross-polarized to co-polarized scattered intensities and the ratio of the same-helicity to the opposite-helicity scattered intensities:

$$\mu_L = \frac{I^{\text{sca}} - Q^{\text{sca}}}{I^{\text{sca}} + Q^{\text{sca}}} = \frac{a_1(\Theta) - a_2(\Theta)}{a_1(\Theta) + 2b_1(\Theta) + a_2(\Theta)}, \quad (9)$$

$$\mu_C = \frac{I^{\text{sca}} + V^{\text{sca}}}{I^{\text{sca}} - V^{\text{sca}}} = \frac{a_1(\Theta) + a_4(\Theta)}{a_1(\Theta) - a_4(\Theta)}. \quad (10)$$

These quantities are used widely in radar and lidar remote sensing [11, 26–28] because they vanish at the exact backscattering direction if multiple scattering is insignificant and the scattering particles are spherically symmetric. Our results demonstrate convincingly that multiple scattering causes an increasingly significant deviation of $\mu_L(180^\circ)$ and $\mu_C(180^\circ)$

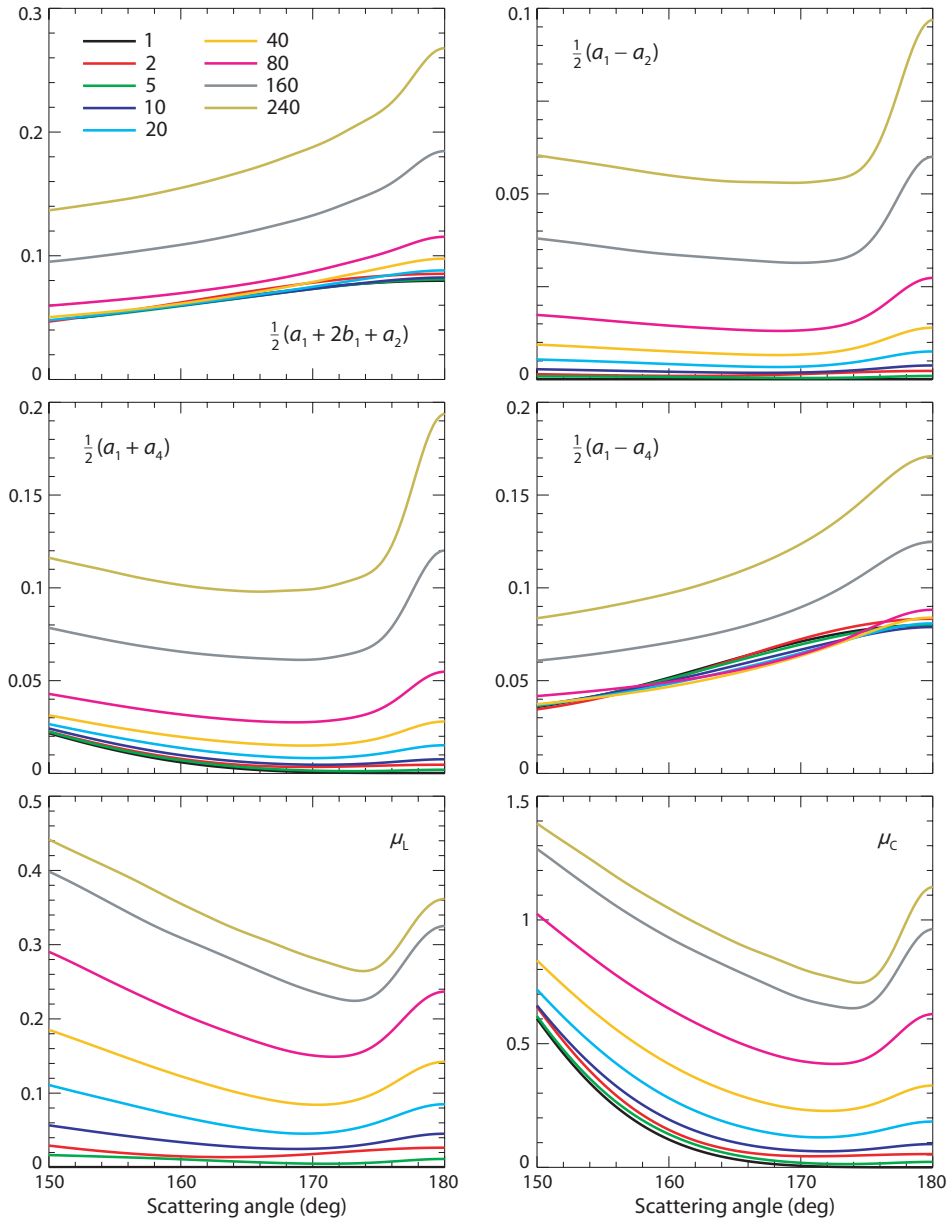


Fig. 10. Polarization characteristics of backscattered light computed for the volume V of discrete random medium filled with $N = 1, \dots, 240$ particles having the same refractive index $m = 1.32$.

from zero, while CB causes pronounced backscattering peaks in the μ_L and μ_C angular profiles. The circular polarization ratio is systematically greater than the linear polarization ratio, which is consistent with the results of CB computations for plane-parallel layers consisting of spherical particles [11].

A legitimate question is whether our results based on averaging over orientations of only one random N -particle configuration are statistically representative of all possible realizations of the N -particle group. In fact, this may not be the case for small values of N , as illustrated by Fig. 6. Somewhat unexpectedly, the red curves corresponding to $N = 2$ deviate from the black single-particle curves more than the green curves corresponding to $N = 5$. The

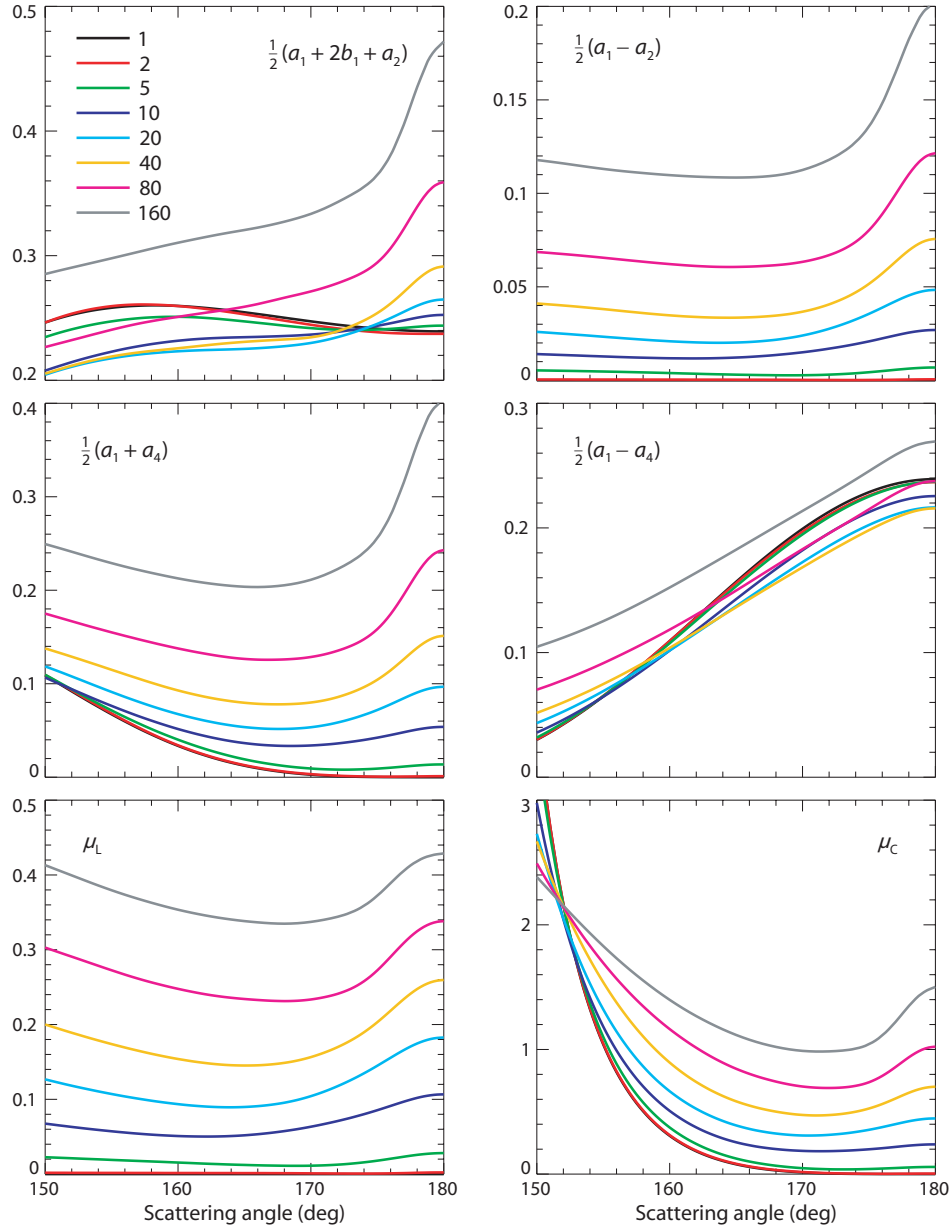


Fig. 11. Polarization characteristics of backscattered light computed for the volume V of discrete random medium filled with $N = 1, \dots, 160$ particles having the same refractive index $m = 1.5$.

explanation of this seemingly strange result is that the particles forming the specific $N = 5$ configuration are widely separated; whereas, the particles forming the $N = 2$ configuration are closely spaced and, thus, interact more efficiently. However, such artifacts become less probable with increasing N so that different random realizations of a many-particle group can be expected to yield virtually the same results. This is illustrated in Fig. 8(b) computed for $N = 160$ and $m = 1.32$.

One manifestation of CB that is not seen in our T -matrix results is the polarization opposition effect (POE) [29]. This effect is observed for media composed of subwavelength-sized particles and illuminated by unpolarized light; it has the same origin as the so-called

azimuthal asymmetry of the backscattering intensity peak in the case of linearly polarized incident light [30]. However, POE causes a much more subtle polarization feature than the backscattering enhancement of intensity [11, 31] and can be masked by the strong negative polarization branch at backscattering angles exhibited by the single-particle curves in Figs. 8(d) and 8(f). Furthermore, it is still unclear whether POE can be produced by wavelength-sized spherical particles like the ones used in our computations [32]. This uncertainty obviously calls for an extension of this study wherein particle size parameters other than 4 are considered.

It is well known that nonspherical particles with large aspect ratios can preserve Rayleigh-like polarization to significantly larger size parameters than volume-equivalent spherical particles [33, 34]. This factor may play a significant role in forming the POE observed for a number of solar system objects [35, 36] and makes desirable an extension of this study to multiple scattering by nonspherical particles (cf. [37, 38]).

6. Discussion

The numerically exact T -matrix computations analyzed in this paper provide a vivid demonstration of the onset and evolution of various multiple-scattering effects with increasing number of particles in a statistically homogeneous scattering volume. These results illustrate and substantiate the methodology underlying the microphysical theories of radiative transfer and CB [11] and should have significant implications for particle characterization and remote sensing research [6–11, 20, 37–42].

It is important to recognize, however, that the very concept of wave phase applies only to transverse waves such as plane and spherical waves and that the concepts of reciprocity and ladder and cyclical diagrams invoked to explain CB and derive RTE are implicitly based on the assumption that each particle in a particle string (Fig. 4) is located in the far-field zones of the previous and the following particle [11]. In other words, one must assume that a wave scattered by a particle develops into a transverse spherical wave by the time it reaches another particle. This assumption is unlikely to be problematic in the case of electromagnetic scattering by sparse discrete random media such as clouds and dilute particle suspensions. However, the stringent criteria of far-field scattering [11] can often be violated in the case of densely packed particles, thereby making more difficult and less definitive the accurate quantitative interpretation of laboratory and remote-sensing measurements of electromagnetic scattering by dense particle suspensions and particulate surfaces.

It is encouraging in this regard that all manifestations of multiple scattering and CB analyzed in the preceding section are consistent, both qualitatively and semi-quantitatively, with those predicted by the asymptotic low-density microphysical theories of radiative transfer and CB [3, 11, 31]. This result indicates that even in densely packed particulate media, the wavelets multiply scattered along strings of widely separated particles still provide a significant contribution to the total scattered signal and make quite pronounced the classical multiple-scattering and CB effects. There is no doubt, however, that definitive quantitative analyses of scattering measurements for densely packed particulate media need to be based on direct solutions of the Maxwell equations. In particular, this study may indicate that the T -matrix approach could eventually be used to model the onset of strong localization of electromagnetic waves which appears to be a rather elusive phenomenon [43–47]. As we have already indicated, the obvious advantage of an approach based on direct and numerically exact solutions of the Maxwell equations is that it can potentially be used to determine all quantitative scattering characteristics of a complex particulate system, including ones that may not be easy to observe.

Acknowledgments

The authors thank Joop Hovenier, Pavel Litvinov, Victor Tishkovets, and Bart van Tiggelen for numerous illuminating discussions. This research was supported by the NASA Radiation Sciences Program managed by Hal Maring.